2-methylfuran pyrolysis: gas-phase modelling and soot formation

Katiuska Alexandrino, Cristian Baena, Ángela Millera, Rafael Bilbao, María U. Alzueta

Aragón Institute of Engineering Research (I3A). Department of Chemical and Environmental Engineering. University of Zaragoza. 50018 Zaragoza. Spain

Corresponding author: María U. Alzueta

Fax: +34976761879, e-mail: uxue@unizar.es

Aragón Institute of Engineering Research (I3A). Department of Chemical and Environmental Engineering. University of Zaragoza. C/ Mariano Esquillor, s/n. 50018 Zaragoza. Spain

Type of article: accepted article

Preference for figures in color: online only

Abstract

Since the recent discoveries in the high efficiency production methods of 2,5-dimethylfuran (2,5-DMF) and 2-methylfuran (2-MF), and due to their good physicochemical properties, these alkylated furan derivatives have been highly considered as fuels or additives in gasoline and diesel engines. However, the cyclic structures of 2,5-DMF and 2-MF may make them effective soot precursors. We have recently studied the capacity of 2,5-DMF to form soot under different pyrolysis experimental conditions, in a flow reactor, and we now focus on the study of the capacity of 2-MF to form soot under the same conditions. In this way, a systematic investigation of the temperature and fuel concentration effects on the soot formed in the 2-MF pyrolysis was undertaken, in an atmospheric-pressure flow reactor, in the temperature range of 975-1475 K, and with 9000 and 18000 ppm of 2-MF (inlet total carbon of 45000 and 90000 ppm, respectively). The increase in the soot yield is favoured by the rise in both the temperature and the inlet 2-MF concentration, while the gas yield decreases as the temperature increases without a noticeable influence of the inlet 2-MF concentration. A gas-phase chemical kinetic model was proposed to describe both the pyrolysis of 2-MF and 2,5-DMF. It was validated against the gas-phase data obtained in this work, as well as with a series of experimental data from literature including shock tube and flow reactors. Results show that 2-MF has a high capacity to form soot, and C4 species play a major role in the formation of intermediates that yield polycyclic aromatic hydrocarbons (PAH), well known as soot precursors. However, the soot yield in the 2-MF pyrolysis was found to be lower than that in the 2,5-DMF pyrolysis, mainly because, according to modelling results, during the 2,5-DMF pyrolysis the cyclopentadienyl radicals are highly formed, whose recombination yields directly naphthalene without any other intermediate.

Keywords**:** 2-methylfuran, pyrolysis, soot, gas-phase, modelling.

1. Introduction

One of the main reasons for proposing alternative fuels, which, depending on their physical and chemical characteristics, can be used blended or not with the conventional fuels [1], is to reduce the strictly regulated particulate matter (PM) emissions, principally from diesel engines. Soot is a major component of PM emitted by engines and it can have adsorbed polycyclic aromatic hydrocarbons (PAH), which exhibit a human health hazard and are known to be the major soot precursors [2].

The latest improvements in the production methods of alkylated furan derivatives, from non-food feedstocks, specifically 2,5-dimethylfuran (C_6H_8O, 2,5-DMF) and 2-methylfuran (C_5H_6O, 2-MF) [e.g. 3-4], have increased the interest of using these compounds as biofuels. Some of the physicochemical properties of 2,5-DMF and 2-MF are similar to those of gasoline and they have a series of attractive features compared to ethanol, the most commonly biofuel used in spark ignition (SI) engines due to its renewable nature and high octane number [5]. These features include: lower latent heat of vaporization, insolubility in water and higher energy density. The 2-MF molecule is more compact than 2,5-DMF and some of its properties, such as its higher research octane number (RON) and its lower boiling point [6], make it more attractive as engine fuel than 2,5-DMF.

2-MF (an intermediate in the 2,5-DMF conversion [7]) has been studied as biofuel mainly in SI engines, showing that 2-MF is compatible with the gasoline engines when is used either as pure fuel [e.g. 8,9] or as gasoline/2-MF blend fuel [6]. Regarding the PM emissions, they seem to be lower in the 2-MF combustion than in the gasoline combustion [9], but higher compared to the PM emissions from ethanol combustion [8]. Furthermore, a more recent study [10] has addressed the use of 2-MF in a direct-injection compression ignition (DICI) engine, suggesting the use of 2-MF as diesel blend fuel because the high octane number of 2-MF hinders its compression ignition in DICI engines when is used as pure fuel. The results from that work showed that, for a 2-MF mass fraction up to 30 %, the hydrocarbon (HC) and soot emissions were reduced over the entire engine loads tested, while for the 2-MF mass fraction of 40 %, the soot emissions were high for low engine loads. On the other hand, the CO and NO_x emissions with 2-MF addition were higher than those of pure diesel fuel, and increased with the increase of 2-MF fraction. This behavior was more noticeable for CO and NO_x at low and at high engine loads, respectively.

The interest of 2-MF as biofuel, linked with the difficulty to evaluate the complex combustion process in engines, leads to the need of performing studies of both 2-MF pyrolysis and oxidation in laboratory scale reactors. At the same time, the development of kinetic models is required in order to describe the 2-MF conversion under different operating conditions. The 2-MF oxidation studies reported in the literature include premixed flames [e.g. 11-13], ignition delay times [e.g. 14,15], laminar burning velocities [e.g. 14,16], and flow reactor [17]. Most of these works include kinetic modelling study in order to describe the 2-MF oxidation process.

While the 2-MF oxidation has been widely studied, the 2-MF pyrolysis has been hardly investigated. 2-MF pyrolysis studies include the work of Grela et al. [18], where the decomposition of furan, 2-MF and 2,5-DMF, in a flow reactor operating at 1 mTorr, was addressed, although experimental concentration profiles were not reported. Lifshitz et al. [19] studied the thermal decomposition of 2-MF in a single pulse shock tube over the temperature range 1100-1400 K. Mole percent profiles of the gases products detected by gas chromatography (GC) were reported, founding CO as the major gas. The recent study of Cheng et al. [20] approaches a 2-MF pyrolysis study in a flow reactor operating in the temperature range of 900-1530 K, at 30 and 760 Torr. The experimental mole fraction profiles of the pyrolysis products, detected by synchrotron vacuum ultraviolet photoionization mass spectrometry (SVUV-PIMS) and GC, were reported. Modelling calculations were also carried out using an updated model of Somers et al. [21], to which Cheng et al. [20] added reactions describing the formation of aromatics, including PAH [22,23].

According to literature studies, 2-MF seems to have a high tendency to form soot, although there is a lack of information on this regard. For example, Moshammer et al. [12], in their work of low-pressure premixed flames, reported that 2-MF has high capacity to form aromatic species, which are PAH precursors, and therefore soot precursors. Tran et al. [11] also mentioned that the low-pressure premixed 2-MF flame has a certain tendency to form PAH. Through simulations, they found that the formation of PAH is considerably enhanced in the 2,5-DMF flame compared to that of 2-MF. Cheng et al. [20] also found in their 2-MF flow reactor experiments that this fuel has a high tendency to form PAH.

Although these works indicate the high tendency of 2-MF to form soot, no research about the quantification of soot from the 2-MF conversion is reported in literature. Thus, in order to extend the

knowledge of the capacity of 2-MF to form soot under well-controlled laboratory experiments, the present study focuses on the quantification of the soot and the main light gases formed during the 2-MF pyrolysis in an atmospheric-pressure flow reactor. PAH are not experimentally quantified in this work; therefore, the concentration values for these species are not reported here. This work is part of the research works about the pyrolysis of furan derivatives that are carried out in our group. The 2,5-DMF pyrolysis was considered in a previous work of our authorship [24], where this fuel was found to have a capacity to form soot comparable to that of acetylene, an important soot precursor. To facilitate the interpretation of the experimental data of the present work, a gas-phase kinetic model has been established by adding a PAH growth mechanism [25] into a furans conversion mechanism [17]. This extended model has been modified in order to properly predict the gases formed during the pyrolysis of both 2-MF ([19,20] and present work) and 2,5-DMF [24,26,27]. Furthermore, the comparison between the capacity of 2-MF and 2,5-DMF to form soot has been carried out, with a discussion supported by a kinetic modelling study.

2. Experimental method

The experiments were performed at 975, 1075, 1175, 1275, 1375, and 1475 K with an inlet 2-MF concentration of 9000 and 18000 ppm (inlet total carbon of 45000 and 90000 ppm, respectively), which are similar to the conditions used in our previous 2,5-DMF pyrolysis study [24].

Details of the flow reactor and pyrolysis set-up used in this work can be found elsewhere [24,28]. Briefly, a quartz flow reactor (45 mm internal diameter and 800 mm in length) is fixed inside a vertical high temperature furnace. The reactor inlet and outlet are cooled by means of an external air flow. The heated isothermal region (reaction zone) of the flow reactor is 160 mm. An initial total flow rate of 1000 mL(STP)/min is kept constant in each experiment, which results in a temperature dependent gas residence time, t_r (s)=4168/T(K), ranging from 2.8 to 4.3 s. The fuel, which is liquid at room temperature, is pumped into a stainless steel tube maintained at 395 K, using a HPLC pump and N_2 as carrier gas. This fuel-N_2 flow is mixed at the reactor inlet with a separate N_2 flow established by a mass flow controller in order to complete the total flow. In each experiment, the desired temperature is programmed in the furnace, and while this temperature is reached, a N_2 flow of 1000 mL(STP)/min is flowing through the reactor. When the

temperature is stable, part of the N_2 flow is changed by the fuel-N_2 flow, starting to count from here the 3 h that the experiment lasts. According to the procedure established by Ruiz et al. [28], this time allows us to collect a significant amount of soot (more than 1 g) in order to carry out later the reactivity study and characterization analysis of the soot.

The soot formed is collected downstream the reactor outlet by a quartz fiber filter with a pore diameter lower than 1 μm. The filter is weighed before and after each experiment in order to quantify the soot deposited in the filter. In this way, the soot amount is obtained by the sum of the soot found on the reactor walls and the soot found in the filter. The experimental uncertainty in soot measurement is estimated as ±1%. The gas product is quenched at the reactor outlet by an external air flow and is analyzed by an Agilent 6890 gas chromatograph equipped with a thermal conductivity detector (TCD) and a flame ionization detector (FID) (accuracy of ±10 ppm). The main light gases quantified were ethylene, acetylene, hydrogen, benzene, methane, carbon monoxide, and carbon dioxide, and the minor gases were 1,3-butadiene, cyclopentadiene, allene, ethylbenzene, and toluene. The reactor inlet is connected to a pressure transducer to monitor the pressure in the system and to ensure that it does not exceed an established limit pressure of 1.3 atm, in order to avoid operational problems.

3. Modelling

3.1 Mechanism description

Simulations were carried out with the Chemkin Pro software [29]. A kinetic model, based on the 2-MF oxidation mechanism used in our previous study [17], was constructed. This mechanism starts from the GADM mechanism [30] to describe the C1-C2 hydrocarbon chemistry, with subsequent modifications and updates [31-34], and adopts the furan and 2,5-DMF sub-mechanisms from Sirjean et al. [35], and the updated 2-MF sub-mechanism proposed by Somers et al. [21]. Reactions of PAH growth, via H-abstraction/C_2H_2-addition (HACA) mechanism and reactions involving resonantly stabilized free radicals, were included in this model by introducing the PAH sub-mechanism used in our dimethyl carbonate pyrolysis study [25], which incorporates the PAH growth up to pyrene proposed by Appel et al. [36] and from pyrene up to coronene proposed by Richter et al. [37]. The thermodynamic data were taken from the

same sources as the original mechanisms. This extended model, as well as the thermodynamic data, are provided in the Supplementary Material.

Although this work is focused on the 2-MF pyrolysis, the extended model has been modified in order to better predict the results of the gases quantified in the pyrolysis of both 2-MF and 2,5-DMF, in this work, as well as in the literature. For this, some reactions concerning many species/radicals and even some PAH were modified/added in the mechanism. The main added (R1-R56) and modified (R57-R86) reactions are reported in Table 1. See Table S1 in the Supplementary Material for details in the name of the species. This final proposed model, containing 469 species and 2118 reactions, is also provided in the Supplementary Material.

Table 1. Main added and modified reactions in the extended model [a].

	Nº	Reaction	A	n	E_a	Reference
Added						
	R1	$H_2CCCH + H_2CCCH \rightleftarrows C_6H_5 + H$	2.02×10^{33}	-6.00	15940	[20]
	R2	$H_2CCCH + C_4H_6 \rightleftarrows C_6H_5CH_3 + H$	6.53×10^{5}	1.28	-4611	[20]
	R3	$H_2CCCH + C_3H_5 \rightleftarrows C_5H_4CH_2 + 2H$	3.26×10^{29}	-5.40	3390	[20]
	R4	$H_2CCCH + HCCO \rightleftarrows C_4H_4 + CO$	2.50×10^{13}	0.00	0	[20]
	R5	$pC_3H_4 + H \rightleftarrows aC_3H_4 + H$ [b]	6.27×10^{17}	-0.91	10079	[20]
	R6	$aC_3H_4 + CH_3 \rightleftarrows H_2CCCH + CH_4$	1.30×10^{12}	0.00	7700	[20]
	R7	$nC_4H_3 + C_2H_2 \rightleftarrows C\text{-}C_6H_4 + H$	6.90×10^{46}	-10.01	30100	[20]
	R8	$iC_4H_3 + H \rightleftarrows C_4H_4$	3.40×10^{43}	-9.01	12120	[20]
	R9	$nC_4H_5 \rightleftarrows C_4H_4 + H$	3.03×10^{11}	0.87	39300	[20]
	R10	$C_4H_4O + H \rightleftarrows CH_2CHCCO + H_2$	7.01×10^{14}	-0.17	8783.2	[20]
	R11	$C_5H_5 + C_4H_2 \rightleftarrows C_9H_7$	2.00×10^{13}	0.00	10000	[20]
	R12	$c\text{-}C_6H_4 + pC_3H_4 \rightleftarrows C_9H_8$	1.00×10^{13}	0.00	10000	[20]
	R13	$C_6H_5 + C_4H_4 \rightleftarrows C_6H_5C_2H + C_2H_3$	3.20×10^{11}	0.00	1350	[20]
	R14	$C_6H_5 + H_2CCCH \rightleftarrows C_9H_7 + H$	2.00×10^{13}	0.00	0	[20]
	R15	$C_6H_5 + H_2CCCH \rightleftarrows C_9H_8$	1.50×10^{75}	-17.80	39600	[20]
	R16	$C_5H_4CH_2 \rightleftarrows C_6H_5 + H$ [b]	2.24×10^{68}	-14.70	142570	[20]
	R17	$C_5H_4CH_2 \rightleftarrows C_6H_6$ [b]	1.45×10^{45}	-8.90	96999	[20]
	R18	$C_5H_4CH_2 + H \rightleftarrows C_6H_6 + H$ [b]	1.66×10^{25}	-2.99	13691	[20]
	R19	$C_7H_5 \rightleftarrows C_4H_2 + H_2CCCH$[b]	8.51×10^{82}	-19.18	125340	[20]
	R20	$C_7H_5 + C_2H_2 \rightarrow C_9H_7$ [b]	2.58×10^{46}	-9.96	39426	[20]
	R21	$C_7H_5 + C_2H_4 \rightleftarrows C_9H_8 + H$	3.124×10^{-6}	4.71	1417.5	[20]
	R22	$C_7H_5 + H_2CCCH \rightleftarrows C_{10}H_8$ [b]	1.07×10^{45}	-9.57	17000	[20]
	R23	$C_6H_5C_2H + CH_3 \rightarrow C_9H_8 + H$	3.00×10^{11}	0.00	7600	[20]
	R24	$C_6H_5C_2H_3 \rightleftarrows C_6H_6 + C_2H_2$	1.58×10^{11}	0.00	58440	[20]
	R25	$C_9H_7 \rightarrow C_7H_5 + C_2H_2$ [b]	1.476×10^{79}	-17.61	162389	[20]
	R26	$C_9H_7 + H$ (+M) $\rightleftarrows C_9H_8$ (+M)	1.00×10^{14}	0.00	0	[20]
		low	4.40×10^{80}	-18.28	12994	
		Troe	0.068 400.7	4135.8	5501.9	
		H_2/2.0/H_2O/6.0/CH_4/2.0/CO/1.5/CO_2/2.0/				
	R27	$C_9H_8 + CH_3 \rightleftarrows C_9H_7 + CH_4$	1.80×10^{-01}	4.00	456.5	[20]
	R28	$2C_2H_2 \rightleftarrows C_4H_2 + H_2$	1.51×10^{13}	0.00	21350	[38]
	R29	$C_6H_4C_2H + C_6H_6 \rightleftarrows C_{14}H_{10} + H$	1.10×10^{23}	-2.92	8010	[38]
	R30	$C_9H_7 + C_5H_5 \rightarrow C_{14}H_{10} + H_2$	4.30×10^{36}	-6.30	22530	[38]
	R31	$C_9H_8 + CH_2S \rightleftarrows C_{10}H_8 + 2H$	4.00×10^{13}	0.00	4370	[38]
	R32	$C_9H_8 + H_2CCCH \rightarrow C_{12}H_8 + H + H_2$	1.55×10^{14}	0.00	25912	[38]
	R33	$C_{10}H_8 + CH_2S \rightleftarrows 1\text{-}C_{10}H_7CH_3$	4.40×10^{13}	0.00	4370	[38]
	R34	$C_{10}H_8 + CH_2S \rightleftarrows 2\text{-}C_{10}H_7CH_3$	4.40×10^{13}	0.00	4370	[38]

	R35	$1\text{-}C_{14}H_9 + C_4H_4 \rightleftarrows C_{18}H_{12} + H$	3.20×10^{33}	-5.70	12750	[38]
	R36	$C_{16}H_9 + C_4H_4 \rightleftarrows C_{20}H_{12} + H$	3.30×10^{33}	-5.70	12750	[38]
	R37	$C_{18}H_{10} + C_2H_2 \rightleftarrows C_{20}H_{12}$	5.10×10^{21}	-3.36	8900	[38]
	R38	$4\text{-}C_{18}H_{11} + H \rightleftarrows C_{18}H_{10} + H_2$	1.00×10^{14}	0.00	0	[38]
	R39	$5\text{-}C_{18}H_{11} + H \rightleftarrows C_{18}H_{10} + H_2$	1.00×10^{14}	0.00	0	[38]
	R40	$pC_3H_4 + H_2CCCH \rightleftarrows C_6H_6 + H$	2.20×10^{11}	0.00	2000	[40]
	R41	$aC_3H_4 + H_2CCCH \rightleftarrows C_6H_6 + H$	2.20×10^{11}	0.00	2000	[40]
	R42	$C_5H_5 + C_4H_4 \rightleftarrows C_9H_8 + H$	0.50×10^{48}	-9.97	36755	[40]
	R43	$C_6H_5C_2H + nC_4H_3 \rightleftarrows C_{10}H_7C_2H_2$	7.51×10^{75}	-17.90	39600	[40]
	R44	$C_9H_7 + H_2CCCH \rightleftarrows C_{12}H_8 + 2H$	8.10×10^{42}	-9.20	15153	[40]
	R45	$C_{10}H_8 + nC_4H_3 \rightleftarrows C_{14}H_{10} + H$	4.00×10^{13}	0.00	15976	[40]
	R46	$1\text{-}C_{14}H_9 + C_2H_2 + C_2H_2 \rightarrow C_{18}H_{12} + H$	1.00×10^{13}	0.00	0	[40]
	R47	$C_{12}H_7 + C_2H_2 \rightleftarrows 4\text{-}C_{14}H_9$	7.00×10^{37}	-8.02	16295.1	[11]
	R48	$1\text{-}C_{14}H_9 + C_2H_2 \rightleftarrows pC_{16}H_{10} + H$	6.60×10^{24}	-3.36	17686	[11]
	R49	$C_{18}H_{12} \rightleftarrows C_2H_2 + pC_{16}H_{10}$	1.00×10^{11}	0.00	89420	[11]
	R50	2,5-DMF $\rightleftarrows C_4H_5\text{-}1S + CH_3CO$ [b,c]	5.52×10^{107}	-26.40	142000	[26]
	R51	$C_6H_5OH \rightleftarrows C_5H_6 + CO$	8.62×10^{15}	-0.61	74115	[26]
	R52	$C_{12}H_{10} \rightleftarrows C_{12}H_8 + H_2$	4.70×10^{13}	0.00	61600	[37]
	R53	$aC_{16}H_{10} \rightleftarrows fC_{16}H_{10}$	8.51×10^{12}	0.00	62860	[37]
	R54	$H_2CCCH + H_2CCCH \rightleftarrows C_5H_4CH_2$ [b]	8.25×10^{46}	-10.10	16900	[39]
	R55	$C_5H_6 + C_5H_5 \rightleftarrows C_6H_6 + nC_4H_5$	5.00×10^{9}	0.00	0	[21]
	R56	$pC_{16}H_{10} \rightleftarrows C_4H_2 + C_{12}H_8$	1.00×10^{11}	0.00	45000	[41]
Modified						
	R57	$CH_4 + H \rightleftarrows CH_3 + H_2$	6.14×10^{5}	2.50	9587	[20]
	R58	$C_2H_3 + CH_3 \rightleftarrows CH_4 + C_2H_2$	3.92×10^{11}	0.00	0	[20]
	R59	$C_2H_3 + C_2H_4 \rightleftarrows C_4H_7\text{-}1$	7.93×10^{38}	-8.47	14220	[20]
	R60	$C_2H_4 + H \rightleftarrows C_2H_3 + H_2$	5.07×10^{7}	1.93	12950	[20]
	R61	$H_2CCCH + H \rightleftarrows pC_3H_4$	1.50×10^{13}	0.00	0	[20]
	R62	$H_2CCCH + H \rightleftarrows aC_3H_4$	2.50×10^{12}	0.00	0	[20]
	R63	$H_2CCCH + CH_2T \rightleftarrows C_4H_4 + H$	5.00×10^{13}	0.00	0	[20]
	R64	$H_2CCCH + CH_3 (+M) \rightleftarrows C_4H_6\text{-}12 (+M)$	1.50×10^{12}	0.00	0	[20]
		low	2.60×10^{57}	-11.94	9770	
		Troe	0.175 1341 60000 9770			
		$H_2/2.0/H_2O/6.0/CH_4/2.0/CO/1.50/CO_2/2.0/C_2H_6/3.0/AR/0.70/$				
	R65	$H_2CCCH + H_2CCCH \rightleftarrows C_6H_6$	1.64×10^{66}	-15.90	27529	[20]
	R66	$pC_3H_4 + H \rightleftarrows H_2CCCH + H_2$	1.30×10^{6}	2.00	5500	[20]
	R67	$iC_4H_3 + H \rightleftarrows C_4H_2 + H_2$	6.00×10^{13}	0.00	0	[20]
	R68	$C_4H_4 + H \rightleftarrows iC_4H_3 + H_2$	3.33×10^{5}	2.53	9240	[20]
	R69	$nC_4H_5 \rightleftarrows C_2H_2 + C_2H_3$ [b]	9.04×10^{44}	-9.65	50910	[20]
	R70	$C_4H_6\text{-}1 \rightleftarrows H_2CCCH + CH_3$ [b]	4.99×10^{81}	-19.37	112156	[20]
	R71	$C_4H_6 + CH_3 \rightleftarrows iC_4H_5 + CH_4$	1.00×10^{14}	0.00	19800	[20]
	R72	$C_6H_5CH_2 + C_2H_2 \rightleftarrows C_9H_8 + H$	3.12×10^{-6}	4.71	1417.5	[20]
	R73	$C_6H_5CH_3 (+M) \rightleftarrows C_6H_5 + CH_3 (+M)$	1.95×10^{27}	-3.16	107447	[20]
		low	1.00×10^{98}	-22.96	122080	
		Troe	0.705 9.99×10^{9} 459 8.21×10^{9}			
	R74	$C_6H_5CH_3 + H \rightleftarrows C_6H_6 + CH_3$	9.49×10^{5}	2.00	944	[20]
	R75	$C_6H_5CH_3 + C_5H_5 \rightleftarrows C_6H_5CH_2 + C_5H_6$	1.60×10^{12}	0.00	15100	[20]
	R76	$C_9H_7 + H_2 \rightarrow C_9H_8 + H$	1.00×10^{12}	0.00	13000	[20]
	R77	$C_9H_8 + H \rightarrow H_2 + C_9H_7$	1.44×10^{7}	2.00	4212.94	[20]
	R78	$C_4H_4 + H \rightleftarrows nC_4H_3 + H_2$	6.65×10^{5}	2.53	12240	[26]
	R79	$C_5H_5 \rightleftarrows H_2CCCH + C_2H_2$	1.27×10^{59}	-13.51	82200	[26]
	R80	$C_5H_5 + C_2H_2 \rightleftarrows C_6H_5CH_2$	3.79×10^{8}	1.50	34420	[26]
	R81	$C_5H_5 + C_5H_5 \rightleftarrows C_{10}H_8 + 2H$	6.39×10^{29}	-4.03	35205.54	[26]
	R82	$C_5H_5CH_3 (+M) \rightleftarrows C_5H_5 + CH_3 (+M)$	1.95×10^{27}	-3.16	107447	[26]
		low	1.00×10^{98}	-22.96	122080	
		Troe	0.705 9.99×10^{9} 459 8.21×10^{9}			
	R83	2,5-DMF + H $\rightleftarrows$ 2-MF + CH_3	1.55×10^{22}	-2.27	13215.5	[26]
	R84	2,5-DMF $\rightleftarrows 5\text{-}C_6H_7O + H$ [b]	2.08×10^{58}	-12.46	110000	[26]
	R85	$C_6H_5 + iC_4H_3 \rightleftarrows C_{10}H_8$	3.18×10^{23}	-3.20	4230	[11]
	R86	$C_6H_5CH_2 + CH_3 \rightleftarrows C_6H_5C_2H_5$	1.19×10^{13}	0.00	221	[11]

[a] Units: s, cm^3, cal, mol.

[b] Reaction in PLOG format. The Arrhenius parameters showed in this table are for 1 atm.

[c] Global reaction of the reaction sequence 2,5-DMF $\rightleftarrows$ 3,4-$C_6H_8O \rightleftarrows C_4H_5\text{-}1S + CH_3CO$.

Most of the rate constants of the reactions in Table 1 were taken from Cheng et al. [20]. Other rate constants from sources regarding the PAH formation and growth in flames of benzene [37]; methane, ethylene, ethane [38-41]; and 2,5-DMF and 2-MF [11] were adopted. Furthermore, some modifications were carried out following the recommendations given by Cheng et al. [26] to better predict the experimental 2,5-DMF data (reactions R50, R51, R83 and R84 in Table 1). It is to be mentioned that, in the present work, we followed the same procedure of Cheng et al. [26] of using the global reaction 2,5-DMF ⇄ C_4H_5-1S + CH_3CO instead of the reaction sequence 2,5-DMF ⇄ 3,4-C_6H_8O ⇄ C_4H_5-1S + CH_3CO to better predict the concentration profile of 2,5-DMF. Considering that this reaction is poorly studied in literature, experiments and more calculations for the rate constant of this global reaction are suggested to further improve the accuracy of the 2,5-DMF kinetics.

The final proposed model is that one used to perform the simulations, as well as, to assess the contribution of different paths to the 2-MF consumption, and the formation and consumption of intermediates, through a rate of production (ROP) analysis at different temperatures, as it will be shown in Section 4 of the present work.

3.2 Mechanism validation against literature data

As it has been mentioned, the proposed model has been built in order to properly predict the pyrolysis of both 2-MF and 2,5-DMF. Table 2 summarizes the pyrolysis works from literature used to validate the proposed mechanism, which include 2-MF and 2,5-DMF pyrolysis studies in a single pulse shock tube and in flow reactors. The experimental data sets cover a wide range of conditions which allow validation of the mechanism.

Table 2. Literature works used to validate the proposed model. SPST: Single pulse shock tube; FR: Flow reactor; t_r: Residence time.

	Reactor type	Fuel (%)	Dilution gas	T (K)	P (atm)	t_r (s)	Reference
2-MF							
Lifshitz et al.	SPST	0.5	Ar	1100-1400[a] 1150-1486[b]	2-3	$2x10^{-3}$	[19]
Cheng et al.	FR	2	Ar	900-1530	0.04 1	$5.3x10^{-3}$-$2.1x10^{-1}$	[20]
2,5-DMF							
Lifshitz et al.	SPST	0.5	Ar	1070-1370[a] 1110-1452[c]	2-3	$2x10^{-3}$	[27]
Cheng et al.	FR	2	Ar	780-1470	0.04 0.2 1	$5.4X10^{-3}$-$2.3X10^{-1}$	[26]
Alexandrino et al.	FR	0.50 0.75 1.50	N_2	975-1475	1	2.8-4.3	[24]

[a] Temperature ranges reported by Lifshitz et al. [19,27] and subsequently corrected by [b] Somers et al. [21] and by [c] Sirjean at al. [35].

The plots comparing the experimental data from literature, and the simulations of the proposed model are shown in Figs. S1-S7, in the Supplementary Material. For comparison, calculations with the models proposed by Cheng for the pyrolysis of 2-MF (Cheng2-MF) [20] and 2,5-DMF (Cheng2,5-DMF) [26] are also represented.

Fig. S1 presents the 2-MF pyrolysis product speciation profiles, expressed in mole percent, from Lifshitz et al. [19] and the simulations of both the model proposed in this work and the Cheng2-MF model. The mole percent of a given species is defined as the ratio between the mole fraction of this species and the sum of all the species mole fractions. The species included in the calculation of the simulated mole percent are the same included in the calculation of the experimental mole percent (those shown in Fig. S1). The temperatures behind the reflected shock wave represented in Fig. S1 are those corrected by Somers et al. [21], where the correlation between the experimental temperatures (T_i) obtained by Lifshitz et al. [19] and the corrected temperature (T_c) is given by T_c (K)=1.12 x T_i (K) - 82.54. Major discrepancies in the fitting between experimental and simulated data are observed for ethane (Fig. S1c), CH_2CO (Fig. S1d), 1,3-butadiene (Fig. S1e), and propene (Fig. S1f).

Figs. S2 and S3 show the experimental and simulated mole fraction profiles of the 2-MF pyrolysis study of Cheng et al. [20], in conjunction with the simulations of the proposed model. It is seen that the

overall agreement between experimental data and simulations of the proposed model can be regarded as acceptable, although this model tends to over-predict once again the propene concentration (Fig. S3j). In spite of the poor prediction of the H_2CCCH radicals (Fig. S2g), the model predicts well the mole fraction profile of benzene (Fig. S3a), which is mainly formed by the recombination of two H_2CCCH radicals in those conditions.

Fig. S4 presents the 2,5-DMF pyrolysis product speciation profiles, expressed in mole percent, from Lifshitz et al. [27], and the simulations of both the proposed and the Cheng2,5-DMF model. The temperatures are those corrected by Sirjean et al. [35] (T_c (K)=1.14 x T_i (K) - 110). The proposed model captures satisfactorily the mole percent trends of the 2,5-DMF and the pyrolysis products, with an under-prediction of 1-butyne (C_4H_6-1) (Fig. S4d), and an over-prediction of the mole percent of cyclopentadiene (C_5H_6) and 2-MF (Fig. S4e). These major discrepancies are also observed with the Cheng2,5-DMF model.

The comparison of the experimental and simulated mole fraction profiles of the 2,5-DMF pyrolysis study of Cheng et al. [26], and simulations by the proposed model, are shown in Figs. S5 and S6. A general good prediction of the experimental data by the proposed model is achieved, although poor predictions are mainly observed for vinylacetylene (Fig. S5b), allyl radicals (Fig. S5l), benzyl radicals (Fig. S6f), phenylacetylene (Fig. S6h), and indenyl radicals (Fig. S6j). It should be noted that, to predict appropriately the mole fraction profile of 2,5-DMF, the important reaction for the 2,5-DMF decomposition, 2,5-DMF ⇄ 3,4-C_6H_8O ⇄ C_4H_5-1S + CH_3CO, was substituted by the global reaction R50, in Table 1, as in Cheng et al. [26], where the carbonaceous intermediate hexa-3,4-dien-2-one (3,4-C_6H_8O) was omitted.

Fig. S7 shows the experimental concentration profiles of the main gases obtained in our previous 2,5-DMF pyrolysis study [24], with the simulation results of both the proposed and the Cheng2,5-DMF models. We used here concentration profiles, instead of the yield profiles published in that work [24], to better appreciate the performance of the models. It is observed that, in general, the trends of all concentration profiles are well captured by the proposed model. On the other hand, the Cheng2,5-DMF model does not predict well the trend of acetylene (Fig. S7d), and the calculated maximum in the benzene concentration profile is shifted about 120 K to higher temperatures (Fig. S7f). It is also observed that the CO_2 concentration is under-predicted by both models, especially from 1175 K. Note that the CO_2

concentration is very low when compared with the rest of species quantified. Figs. S1-S7 allow to verify that the proposed model predicts reasonably well experimental data for the pyrolysis of both 2-MF and 2,5-DMF. Thus, the mechanism validation for the experimental data of the present work will be shown in the next section together with the analysis of the results.

4. Results and discussion

In this section, the soot and gas yields obtained in the 2-MF pyrolysis are shown. The gas-phase products are examined by means of a rate of production (ROP) analyses at different temperatures, using the proposed model. Comparison of soot yields obtained in the pyrolysis of 2-MF and 2,5-DMF is done, and their capacities to form soot are discussed through kinetic analysis.

Soot and gas yields

Figure 1 shows the soot and gas yields (in %), i.e., the carbon in soot (around 98 %wt. of the soot amount) and gases, respectively, relative to the total carbon amount fed into the reactor, as a function of temperature, obtained in the pyrolysis of 9000 and 18000 ppm of 2-MF. The sum of both yields is not 100% because by-products, such as a condensate and pyrolytic carbon, which formation cannot be avoided, are generated but not quantified. Moreover, the no quantification of some intermediates species that can be produced during the pyrolysis processes may also contribute to this fact.

It is observed that, as both the temperature and the inlet 2-MF concentration increase, so does the soot yield, reaching values around 44 and 52.4 % for 9000 and 18000 ppm of 2-MF, respectively. The influence of the inlet 2-MF concentration on the soot yield is only pronounced at temperatures higher than 1275 K. On the other hand, the gas yield decreases with increasing temperature, because the reactions leading to the formation of soot and soot precursors are favoured at high temperatures and therefore the carbon is converted to soot instead to gases. There is not a notable effect of the inlet 2-MF concentration on the gas yield.

As happened in our 2,5-DMF pyrolysis study [24], three events are seen to occur during the 2-MF pyrolysis:

1. In the experiments carried out at 1075 and 1175 K, with the two inlet 2-MF concentrations studied, a brown liquid was formed. In this way, the soot yields at 1075 and 1175 K, shown in Fig. 1, should be considered with caution because the formation of the condensate may affect the quantification of soot since part of it could be deposited in the filter. The condensate obtained with 9000 ppm of 2-MF at 1075 K was qualitatively analyzed using a 7890A gas chromatograph coupled to a MSD 5975C mass selective detector of Agilent Technologies, finding that this condensate is composed by several PAH, which are the same as were found in the condensate formed in the 2,5-DMF pyrolysis [24]. These PAH are shown in Table S2 in the Supplementary Material.

2. It is believed that soot has not been yet formed at 1075 K because no soot was found on the reactor walls at this temperature. In this way, the soot yields at 1075 K, shown in Fig. 1, correspond in fact to the condensate deposited in the filter. Thus, 1175 K is considered the lower temperature for soot formation corresponding to the temperature values studied in this work.

3. In the experiment performed with 18000 ppm of 2-MF at 1175 K, the pressure in the system went up over the pressure limit (1.3 atm) after 2 h of experiment, forcing to stop the experiment. As the experiments are performed in stationary conditions, the soot yield at 1175 K for 18000 ppm of 2-MF, shown in Fig. 1, corresponds to the soot mass extrapolated at 3 h.

Gas-phase analysis

The experimental and 2-MF conversions for 9000 and 18000 ppm of 2-MF are represented in Fig. 2. in conjunction with the calculated 2-MF conversions with the proposed model. For comparison, the calculated 2-MF conversions with the model proposed by Cheng et al. [20], for the 2-MF pyrolysis, are also represented. It is observed that the simulated conversions by the two models are in good agreement with the experimental data. The 2-MF conversion starts at around 900 K and is total around 1175 K, and there is not a noticeable influence of the inlet 2-MF concentration on this conversion.

As it has been mentioned above, ROP analysis has been performed at different temperatures. The reaction flux diagram for 2-MF pyrolysis at 1000 K (2-MF conversion of approximately 50 %) is presented in

Fig. 3. The main path for the 2,5-DMF conversion is also shown in Fig. 3 for further discussion when the comparison between the capacity of 2-MF and 2,5-DMF to form soot is made later.

The 2-MF consumption is dominated by (1) H-abstraction reactions from the methyl side of 2-MF by H atoms, and methyl (CH_3) and vinyl (C_2H_3) radicals, representing the main path to the formation of hydrogen, methane and ethylene, respectively, (Path 1), and by (2) H-addition at C5 of the furan ring and a subsequent ring opening (Path 2).

The H-abstraction reactions (path 1 in Fig. 3) yield to the intermediate 2-furanylmethyl radical (C_5H_5O). Its ring opening produces the 3,4-pentadiene-1-one-2-yl radical ($H_2CCCHC^{\bullet}HCHO$), which yields its secondary conformer ($H_2CCCHC^{\bullet}HCOH$). This last radical can undergo a 1 → 4 intramolecular hydrogen atom transfer reaction to finally form the radical $H_2CCHC^{\bullet}HCHCO$, which isomerizes to $H_2CCHCHCHC^{\bullet}O$. The following decarbonylation yields the n-butadienyl radical (nC_4H_5) and CO. In this way, the H-abstraction from 2-MF is the main source of nC_4H_5 radicals, which decomposition triggers the formation of effective soot precursors: (1) vinylacetylene (C_4H_4) and H atoms, and (2) acetylene and the vinyl radicals. Vinylacetylene mainly reacts with vinyl radicals to form benzene and H atoms, representing the principal via for the benzene formation and vinyl radicals consumption. Vinylacetylene may also react with H_2CCCH radicals or combine with itself to form benzyl radicals and styrene, respectively. Thus, these aromatics (benzene, benzyl radicals, and styrene) lead to the formation of naphthalene, with ethylbenzene ($C_6H_5C_2H_5$), 1-phenylethyl radicals (C_8H_9), and phenylvinyl radicals ($C_6H_5C_2H_2$) as intermediates. Among these paths to the naphthalene formation, the dominant one is the combination of two vinylacetylene (C_4H_4) to give styrene ($C_6H_5C_2H_3$) followed by its H-abstraction by methyl radicals to give phenylvinyl ($C_6H_5C_2H_2$) radicals which, by the HACA mechanism, finally produce naphthalene.

On the other hand, the H-addition at 2-MF (path 2 in Fig. 3), which is a reaction that gains more importance with increasing temperature, originates the ring opening and forms the $H_3CCOC^{\bullet}HCHCH_2$ radical, which demethylation gives vinyl ketene (C_4H_4O) and methyl radicals. C_4H_4O mainly reacts by ring closure to form cyclohexa-2,5-dien-1-one (2,5-C_6H_6O) leading to further formation of cyclohexa-2,4-dien-1-one (2,4-C_6H_6O) via formation of the biradical BiC_6H_6O. 2,4-C_6H_6Oreacts , via a concerted reaction, into phenol (C_6H_5OH), which in turn reacts with methyl radicals and by CO elimination to form phenoxy radicals

and cyclopentadiene, respectively. The phenoxy radicals and cyclopentadiene finally yield cyclopentadienyl radicals, where the H-abstraction from cyclopentadiene by methyl radicals is the main via to the formation of cyclopentadienyl radicals in these conditions.

As it was mentioned above, the H-abstraction reactions from the methyl side of 2-MF by vinyl and methyl radicals (path 1 in Fig. 3) represent the main via to the formation of ethylene and methane, two of the major gases found in this work. Fig. 4 shows the experimental and modelled concentration profiles of these species, as a function of temperature, for both inlet 2-MF concentrations. It is observed a maximum in both experimental concentration profiles at around 1075-1175 K. Both the proposed and the Cheng2-MF models predict quite well the concentration trends of both species. However, the CH_4 maximum calculated by the Cheng2-MF model is shifted to about 75 K less (Fig. 4b). Moreover, both models under-predict the CH_4 concentration at temperatures higher than 1175 K, with a greater under-prediction by the Cheng2-MF model.

At temperatures higher than 1075 K, a high 2-MF conversion is obtained (Fig. 2). Thereby, the H-abstraction reactions from 2-MF become negligible for the formation of C_2H_4 and CH_4. Thus, the reactions involving intermediate species become the main routes to the formation of these species, such as the reaction of 1,3-butadiene with H atoms to form C_2H_4 (reaction R87), and the reaction of methyl radicals with indene (reaction R27, in Table 1) and with cyclopentadiene (reaction R88, path 2 in Fig. 3) to form CH_4.

$C_4H_6 + H \rightleftarrows C_2H_4 + C_2H_3$ (R87)

$CH_3 + C_5H_6 \rightleftarrows C_5H_5 + CH_4$ (R88)

At temperatures higher than 1175 K, the C_2H_4 concentration decreases due to its consumption to give C_2H_3 radicals which subsequently form C_2H_2, while the CH_4 concentration decreases due to the competitive reactions consuming CH_3 radicals which lead to the formation of PAH.

1,3-butadiene (C_4H_6) and cyclopentadiene (C_5H_6), species involved in the formation of C_2H_4 (reaction R87) and CH_4 (reaction R88), respectively, were two of the minor gases quantified in this work. Their experimental and predicted concentration profiles, for both inlet 2-MF concentrations, are reported in Fig. 5. This figure also reports the other three minor gases (allene, ethylbenzene and toluene) quantified in this work. These species were only detected at 975 and 1075 K. It can be observed that both the proposed and

Cheng2-MF models predict a maximum in each concentration profile, which are located in the 975-1100 K temperature range.

Calculations indicate that the 1,3-butadiene formation is mainly controlled by C4 radicals (reactions R89-R91), while reactions involving the consumption of phenol (reactions R51, in Table 1, and R92) are the main sources of cyclopentadiene formation.

$CH_3C^{\bullet}HCHCH_2 \rightleftarrows C_4H_6 + H$ (R89)

$C^{\bullet}H_2CH_2CHCH_2 \rightleftarrows C_4H_6 + H$ (R90)

$iC_4H_5 + aC_3H_4 \rightleftarrows C_4H_6 + H_2CCCH$ (R91)

$C_6H_5OH + C_5H_5 \rightleftarrows C_6H_5O + C_5H_6$ (R92)

On the other side, the allene formation is mainly controlled by reaction R5 in Table 1, and the formation of ethylbenzene and toluene are controlled by the reaction of benzyl radicals with methyl radicals (reaction R86, in Table 1) and with cyclopentadiene (reaction -R75, in Table 1), respectively.

Benzene, acetylene and hydrogen are important species involved in the HACA mechanism. These species were among the major species found in this work. Their experimental and modelled concentration profiles, as a function of temperature, are plotted in Fig. 6. While a maximum, at approximately 1075-1175 K, is observed in the experimental concentration profiles of benzene and acetylene (Figs. 6a and 6b, respectively), the hydrogen concentration increases with increasing temperature, with a more noticeable increment from 1175 K (Fig. 6c).

Both models capture the benzene concentration maximum, although the Cheng2-MF model shifts it approximately 45 K to lower temperature (Fig. 6a). On the other hand, the calculated concentration of acetylene by the Cheng2-MF model increases with increasing temperature, not describing its maximum. This maximum can be well captured by the proposed model, although the calculated concentration increases above 1375 K, which is not observed experimentally (Fig. 6b).

The proposed model satisfactorily predicts the hydrogen concentrations, while the Cheng2-MF model under-predicts these concentrations, especially with 18000 ppm of 2-MF from 1275 K (Fig. 6c)

The formation of benzene, acetylene, and hydrogen at low temperature (approximately 1000 K) proceeds through path 1 in Fig. 3, i.e., the reaction of vinylacetylene with vinyl radicals, the decomposition of n-butadienyl radicals, and the H-abstraction from the methyl side of 2-MF by H atoms, respectively.

At approximately 1075 K, the benzene production continues to be mostly dominated by the same reaction, while both the decomposition of the vinyl radicals (reaction R93) and the reaction of propyne with H atoms (reaction R94) dominate the acetylene production.

$C_2H_3 (+M) \rightleftarrows C_2H_2 + H (+M)$ (R93)

$pC_3H_4 + H \rightleftarrows C_2H_2 + CH_3$ (R94)

At this temperature, the recombination of two acetylene molecules (reaction R28 in Table 1) and the reaction between indenyl and cyclopentadienyl radicals (reaction R30, in Table 1) mainly dominate the hydrogen production.

Benzene is consumed from around 1175 K by reaction R95 due to the increase in the concentration of H atoms with the increase of the temperature.

$C_6H_6 + H \rightleftarrows C_6H_5 + H_2$ (R95)

This reaction originates the reaction sequence shown in Fig. 7, which involves the main reactions for the acetylene consumption at high temperatures (reactions R32, in Table 1, and R96).

$C_2H_2 + C_{20}H_{11} \rightleftarrows C_{22}H_{12} + H$ (R96)

The inclusion of reactions R28 (important reaction for the C_2H_2 consumption through the entire temperature range studied) and R37, in Table 1, and R96 in the proposed model, could explain its capacity to predict the acetylene consumption at high temperatures. In the same way, with the increase of the temperature, reactions R77 and R57, in Table 1, become the main routes for molecular hydrogen formation.

CO was the major carbonaceous gas product found in the 2-MF pyrolysis. The CO concentration increases with temperature (Fig. 8a), keeping a constant concentration above 1175 K, for both inlet 2-MF concentrations. CO formation, at approximately 1000 K, occurs by the decomposition of the $H_2CCHCHCHC^{\bullet}O$ radicals (path 1 in Fig. 3). Reaction R51 in Table 1 also gains importance in the CO formation with the increase of temperature. CO oxidizes at high temperatures to CO_2 by reaction R97.

$CO + OH \rightleftarrows CO_2 + H$ (R97)

The CO_2 concentration increases experimentally with increasing temperature (Fig. 8b). However, neither the proposed model nor the Cheng2-MF model can reproduce this tendency, and the CO_2 concentration decreases from 1175 K.

As it has been observed, the gas-phase mechanism proposed matches well the experimental concentration profiles of the species measured in this work. However, due to the non-inclusion of the mass growth process in this mechanism, a direct comparison between experimental and predicted soot mass is not possible. Instead of this, a comparison of the experimental soot mass with the total carbon mass in PAH computed (up to coronene), as a function of temperature for the two inlet 2-MF concentrations studied, is shown in Fig. 9. It is clear that the calculated PAH mass over-estimates the experimental soot amount. This discrepancy can be attributed to the fact that we are maybe considering the mass of PAH that have not really been converted to soot yet at these conditions. Additionally, uncertainties in both the rate coefficients of reactions involved in the PAH growth mechanism and thermodynamic data of PAH may be present as well.

Comparison between the capacity of 2-MF and 2,5-DMF to form soot

When compared with other biofuels, as for example dimethyl carbonate [25], 2-MF shows a higher capacity to form soot under pyrolytic conditions. However, this capacity was found to be lower than the capacity of 2,5-DMF to form soot. Fig. 10 shows the soot yield obtained in the pyrolysis of 2-MF and 2,5-DMF [24], for an inlet total carbon amount of 45000 and 90000 ppm and the same residence time, t_r(s)=4168/T(K). From 1275 to 1475 K, the soot yield in the 2-MF pyrolysis was lower than in the 2,5-DMF case, for both inlet total carbon amounts, by a factor of approximately 1.2. A clear observation can not be made at 1175 K due to the formation of the condensate in both pyrolysis.

The higher capacity of 2,5-DMF to form soot could be explained through an analysis of the dominant paths for the consumption of both fuels during their pyrolysis (Fig. 3). While 2-MF is mainly converted to n-butadienyl radicals, which ultimately form benzene, benzyl radicals, styrene and acetylene (Path 1 in Fig. 3), 2,5-DMF is mainly converted to 2-C_6H_7O radicals to finally form cyclopentadienyl radicals through a series of reactions which include H-abstraction, ring enlargement and β-scission reactions (path

in the right side of the Fig. 3). Although both the 2,5-DMF and 2-MF conversion lead to the formation of important soot precursors, it is known the high ability of cyclopentadienyl radical to the self-combination, where naphthalene is directly formed without any other intermediate [42] (Path 2 in Fig. 3).

To our knowledge, there are not reports in the literature indicating that cyclopentadienyl radicals have been detected in the experimental conversion of 2-MF. However, it is observed in Fig. 3 that these radicals could be formed in the 2-MF pyrolysis by the Path 2, mainly by the H-abstraction from cyclopentadiene by CH_3 radicals. The cyclopentadienyl radicals were not quantified in this work. Thus, a comparison of the experimental concentration profile of the cyclopentadienyl radicals in the pyrolysis of 2-MF and 2,5-DMF can not be performed. However, Fig. 11 shows the calculated concentration profiles of cyclopentadienyl radicals for the pyrolysis of 2-MF and 2,5-DMF, for an inlet total carbon amount of 45000 and 90000 ppm, using the proposed model and, for comparison, the Cheng2-MF and Cheng2,5-DMF models.

It is observed that both the proposed model and the Cheng models predict a higher formation of C_5H_5 radicals in the 2,5-DMF pyrolysis. This result agrees with that observed in the 2,5-DMF and 2-MF flames study of Tran et al. [11], where a calculated mole fraction profile for C_5H_5 was plotted showing that the C_5H_5 radicals are formed 50 times more in the 2,5-DMF flame than in the 2-MF flame.

It is noticeable in Fig. 11 a high discrepancy between the calculations from the proposed model and those from the Cheng models, especially for 2,5-DMF, where the prediction of the concentration of the C_5H_5 radicals is much higher by the Cheng2,5-DMF model than by the proposed model. On the basis of ROP analysis, reaction R88 was identified in both models, as the main reaction for the formation of C_5H_5 radicals in the 2,5-DMF pyrolysis, with a rate constant of $3.51 \times 10^3\, T(K)^{2.866} \exp(-2846/T(K))$ $cm^3\ mol^{-1}\ s^{-1}$ in the two models. However, while in the proposed model the reaction R55, in Table 1, was found to be the main path for the consumption of C_5H_5 radicals, in the Cheng2,5-DMF model the main path was the H-abstraction reaction R98.

$$2,5\text{-DMF} + C_5H_5 \rightleftarrows 5\text{-}C_6H_7O + C_5H_6 \qquad \text{(R98)}$$

It is quite possible that the higher concentrations of C_5H_5 radicals by the Cheng2,5-DMF model are due to the reaction R55 in Table 1. While in the proposed model the rate constant of this reaction is 5×10^9

cm^3 mol^{-1} s^{-1} (taken from Somers et. al [21]), in the Cheng2,5-DMF model it is 1.49 x 10^{29} $T(K)^{-4.515}$ exp(-20568/T(K)) cm^3 mol^{-1} s^{-1} (taken from Cavallotti et al. [43]). This means that the rate of reaction R55 in the Cheng2,5-DMF model is much more lower than that in the proposed model, throughout the temperature range studied, which results in a lower consumption of the cyclopentadienyl radicals and therefore in higher concentrations of them.

The effect of the rate constant of this reaction on the calculated concentration profile of the C_5H_5 radicals by the Cheng2,5-DMF model is shown in Fig. 12. It is observed that, when the rate constant of reaction R55 in the Cheng2,5-DMF model is replaced by the rate constant in the proposed model, the concentration of C_5H_5 radicals decreases significantly for both inlet 2,5-DMF concentrations studied, supporting the above mentioned that the higher concentration of C_5H_5 radicals by the Cheng2,5-DMF model can be due to the rate of this reaction.

Since the C_5H_5 radicals were not experimentally quantified in the present work, and given that in the pyrolysis of both 2-MF and 2,5-DMF, the main path for the formation of these radicals is the cyclopentadiene conversion (reaction R88, Path 2 in Fig. 3), it would be interesting to compare the cyclopentadiene concentration profiles found in both pyrolysis. Fig. 13 shows the comparison. It is verified that this species is formed in greater quantities during the 2,5-DMF pyrolysis than during 2-MF pyrolysis, which thus increases the formation of the C_5H_5 radicals. In the work of Tran et al. [11] it was also found, experimentally and by modelling, that the formation of cyclopentadiene is much higher in the 2,5-DMF flame (by a factor of about 20) than in the 2-MF flame. Thus, the increase in the C_5H_5 radicals concentration during the 2,5-DMF pyrolysis activates the direct via to the naphthalene formation by the self-combination of these radicals, as it can be seen in Fig. 3, enhancing the soot formation process.

The explanation given in this work for the higher capacity of 2,5-DMF with respect to 2-MF to form soot, is based on modelling calculations. A deeper investigation, mainly focused on the experimental PAH formation from the pyrolysis of both furans, would be of great help to keep increasing the knowledge of the capacity of these furans to form soot.

The results of the 2-MF sooting tendency from this work, and from low-pressure premixed [11,12,20] and counter-flow diffusion flames [44] studies, could point out 2-MF as a non-environment-

friendly renewable fuel. However, the results of the study of an ethylene atmospheric-pressure premixed flame [13] doped with furans, as well as certain studies in engines [8-10], suggest that the capacity of 2-MF to reduce soot emissions might be more related to its physicochemical properties, combustion characteristics and operating conditions than to its molecular structure. In this way, more comprehensive experimental and kinetic model studies, mainly focused on the tendency to form soot of mixtures of 2-MF with, for example, ethylene, acetylene, gasoline and diesel surrogates, are desirable in both laboratory scale and engines, in order to get a deep insight on the phenomena that decrease the soot emissions when 2-MF is used in engines.

5. Conclusions

The capacity of 2-MF to form soot has been studied through its pyrolysis in an atmospheric-pressure flow reactor, focusing on the influence of the temperature and the inlet 2-MF concentration on the soot and gas formation. Soot was formed from around 1175 K for both inlet 2-MF concentrations considered. The results demonstrate that the soot yield in the 2-MF pyrolysis is high and it is favoured with the increase of both the temperature and the inlet 2-MF concentration, reaching a soot yield value of around 52 % for the higher temperature studied (1475 K) and 2-MF concentration (18000 ppm). On the other hand, while the gas yield decreases with increasing temperature, the inlet 2-MF concentration does not seem to have a noticeable influence on it.

A gas phase kinetic model was used to predict the pyrolysis of both unsaturated cyclic ethers, 2-MF and 2,5-DMF. The model was validated with different pyrolysis experimental data from literature, as well as with the experimental data obtained in this investigation. In general, the proposed model describes satisfactorily the experimental data from literature, as well as the concentration profile of the main gases quantified in this work, and even properly computes the maximum value of acetylene, as it includes key reactions for the consumption of this species at high temperatures. However, a comparison of experimental soot mass with the total PAH mass computed (up to coronene) shows that the PAH mass over-predicts the soot amount, which could be attributed to the fact that we are maybe considering the mass of some PAH that have not really been converted to soot yet at these conditions. Additionally,

uncertainties in the rate coefficients of reactions involved in both the PAH growth mechanism and the thermodynamic data of PAH may be present as well.

The soot yield was found to be lower in the 2-MF pyrolysis than in the 2,5-DMF pyrolysis by a factor of approximately 1.2. This trend could thus mainly be a consequence of the different conversion processes of these two fuels. While in the 2-MF pyrolysis the PAH formation, and consequently soot formation, is favoured mainly through the C4 species ($nC_4H_5 \rightarrow C_4H_4 \rightarrow C_6H_5C_2H_3 \rightarrow C_6H_5C_2H_2 \rightarrow C_{10}H_8$), in the 2,5-DMF pyrolysis the cyclopentadienyl radicals is highly formed, whose self-combination leads to the direct formation of naphthalene without any other intermediate. Although modelling calculations show that the formation of cyclopentadienyl radicals also occurs in the 2-MF pyrolysis, their calculated concentration is greater in the 2,5-DMF pyrolysis. Furthermore, both the experimental and modelling data indicate a greater formation of cyclopentadiene in the 2,5-DMF pyrolysis, whose conversion is the main path for the formation of the cyclopentadienyl radicals. More experimental investigation on the PAH formation from the pyrolysis of both furans is desirable in order to keep increasing the knowledge of the capacity of these furans to form soot.

Moreover, more studies, mainly focused on the tendency to form soot of mixtures of 2-MF with ethylene, acetylene, gasoline and diesel surrogates, is desirable in both laboratory scale (pyrolysis and oxidation experiments) and engines, in order to get a deep insight on the phenomena that decrease the soot emissions when 2-MF is used in engines.

Acknowledgements

Authors are grateful for the financial support from the Aragón Government and European Social Fund (GPT group), and MINECO and FEDER (Project CTQ2015-65226). Ms. K. Alexandrino acknowledges to MINECO the pre-doctoral grant awarded (BES-2013-063049).

References

[1] A.K. Agarwal, Biofuels (alcohols and biodiesel) applications as fuels for internal combustion engines, Prog. Energy Combust. 33 (2007) 233-271.

[2] H. Wang, Formation of nascent soot and other condensed-phase materials in flames, Proc. Combust. Inst. 33 (2011) 41-67.

[3] Y. Roman-Leshkov, C.J. Barret, Z.Y. Liu , J.A. Dumesic, Production of dimethylfuran for liquid fuels from biomass-derived carbohydrates, Nature 447 (2007) 982–985.

[4] X. Tong, Y. Ma, Y. Li, Biomass into chemicals: conversion of sugars to furan derivatives by catalytic processes, Appl. Catal. A-Gen 385 (2010) 1-13.

[5] J. Goldemberg, The challenge of biofuels, Energy Environ. Sci. 1 (2008) 523-525.

[6] H. Wei, D. Feng, G. Shu, M. Pan, Y. Guo, D .Gao, W. Li, Experimental investigation on the combustion and emissions characteristics of 2-methylfuran gasoline blend fuel in spark-ignition engine, Appl. Energy 132 (2014) 317-324.

[7] K.P. Somers, J.M. Simmie, F. Gillespie, C. Conroy, G. Black, W.K. Metcalfe, F. Battin-Leclerc, P. Dirrenberger, O. Herbinet, P.A. Glaude, P. Dagaut, C. Togbé, K. Yasunaga, R.X. Fernandes, C. Lee, R. Tripathi, H.J. Curran, A comprehensive experimental and detailed chemical kinetic modelling study of 2,5-dimethylfuran pyrolysis and oxidation, Combust. Flame 160 (2013) 2291-2318.

[8] M. Thewes, M. Muether, S. Pischinger, M. Budde, A. Brunn, A. Sehr, P. Adomeit, J. Klankermayer, Analysis of the impact of 2-methylfuran on mixture formation and combustion in a direct-injection spark-ignition engine, Energy Fuels 25 (2011) 5549-5561.

[9] C. Wang, H. Xu, R. Daniel, A. Ghafourian, J.M. Herreros, S. Shuai, X. Ma, Combustion characteristics and emissions of 2-methylfuran compared to 2,5-dimethylfuran, gasoline and ethanol in a DISI engine, Fuel 103 (2013) 200-211.

[10] H. Xiao, P. Zeng, Z. Li, L. Zhao, X. Fu, Combustion performance and emissions of 2-methylfuran diesel blends in a diesel engine, Fuel 175 (2016) 157-163.

[11] L.S. Tran, B. Sirjean, P.A. Glaude, K. Kohse- Höinghaus, F. Battin-Leclerc, Influence of substituted furans on the formation of polycyclic aromatic hydrocarbons in flames, Proc. Combust. Inst. 35 (2015) 1735-1743.

[12] K. Moshammer, A. Lucassen, C. Togbé, K. Kohse- Höinghaus, N. Hansen, Formation of oxygenated and hydrocarbon intermediates in premixed combustion of 2-methylfuran, Z. Phys. Chem. 229 (2015) 507-528.

[13] M. Conturso, M. Sirignano, A. D´Anna, Effect of biofuels on particle formation in premixed ethylene-air flames: an experimental study, Fuel 175 (2016) 137-145.

[14] K.P. Somers, J.M. Simmie, F. Gillespie, U. Burke, J. Connolly, W.K. Metcalfe, F. Battin-Leclerc, P. Dirrenberger, O. Herbinet, P.A. Glaude, H.J. Curran, A high temperature and atmospheric pressure experimental and detailed chemical kinetic modelling study of 2-methylfuran oxidation, Proc. Combust. Inst. 34 (2013) 225-232.

[15] N. Xu, Y. Wu, C. Tang, P. Zhang, X. He, Z. Wang, Z. Huang, Experimental study of 2,5-dimethylfuran and 2-methulfuran in a rapid compression machine: comparison of the ignition delay times and relativity at low to intermediate temperature, Combust. Flame 168 (2016) 216-227.

[16] X. Ma, C. Jiang, H. Xu, S. Shuai, H. Ding, Laminar burning characteristics of 2-methylfuran compared with 2,5-dimethylfuran and isooctane, Energy Fuels 27 (2013) 6212-6221.

[17] K. Alexandrino, Á. MIllera, R. Bilbao, M.U. Alzueta, 2-methylfuran oxidation in the abscense and presence of NO, Flow Turbul. Combust. 96 (2016) 343-362.

[18] M.A. Grela, T. Amorebieta, A.J. Colussi, Very low pressure pyrolysis of furan, 2-methylfuran, and 2,5-dimethylfuran. The stability of the furan ring, J. Phys. Chem. 89 (1985) 38-41.

[19] A. Lifshitz, C. Tamburu, R. Shashua, Decomposition of 2-methylfuran. Experimental and modeling study, J. Phys. Chem. A 101 (1997) 1018-1029.

[20] Z. Cheng, S. He, L. Xing, L. Wei, W. Li, T. Li, B. Yan, W. Ma, G. Chen, Experimental and kinetic modeling study of 2-methylfuran pyrolysis at low and atmospheric pressures, Energy Fuels 31 (2017) 896-903.

[21] K.P. Somers, J.M. Simmie, W.K. Metcalfe, H.J. Curran, The pyrolysis of 2-methylfuran: a quantum chemical, statistical rate theory and kinetic modelling study, Phys. Chem. Chem. Phys. 16 (2014) 5349-5367.

[22] Y.Y. Li, J.H. Cai, L.D. Zhang, T. Yuan, K.W. Zhang, F. Qi, Investigation on chemical structures of premixed toluene flames at low pressure, Proc. Combust. Inst. 33 (2011) 593-600.

[23] W.H. Yuan, Y.Y. Li, P. Dagaut, J.Z. Yang, F. Qi, Investigation on the pyrolysis and oxidation of toluene over a wide range conditions. I. Flow reactor pyrolysis and jet stirred reactor oxidation. Combust. Flame 162 (2015) 3-21.

[24] K. Alexandrino, P. Salvo, Á. Millera, R. Bilbao, M.U. Alzueta, Influence of the temperature and 2,5-dimethylfuran concentration on its sooting tendency, Combust. Sci. Technol. 188 (2016) 651-666.

[25] K. Alexandrino, J. Salinas, Á. Millera, R. Bilbao, M.U. Alzueta, Sooting propensity of dimethyl carbonate, soot reactivity and characterization, Fuel 183 (2016) 64-72.

[26] Z. Cheng, L. Xing, M. Zeng, W. Dong, F. Zhang, F. Qi, Y. Li, Experimental and kinetic modeling study of 2,5-dimethylfuran pyrolysis at various pressures, Combust. Flame 161 (2014) 2496-2511.

[27] A. Lifshitz, C. Tamburu, R. Shashua, Thermal decomposition of 2,5-dimethylfuran, Experimental results and computer modeling, J. Phys. Chem. A 102 (1998) 10655-10670.

[28] M.P. Ruiz, A. Callejas, Á. Millera, M.U. Alzueta, R. Bilbao, Soot formation from C_2H_2 and C_2H_4 pyrolysis at different temperatures, J. Anal. Appl. Pyrol. 79 (2007) 244-251.

[29] CHEMKIN-PRO 15131, Reaction Design, San Diego 2013.

[30] P. Glarborg, M.U. Alzueta, K. Dam-Johansen, J.A. Miller, Kinetic modeling of hydrocarbon/nitric oxide interactions in a flow reactor, Combust. Flame, 115 (1998) 1-27.

[31] P. Glarborg, M. Østberg, M.U. Alzueta, K. Dam-Johansen, J.A. Miller, The recombination of hydrogen atoms with nitric oxide at high temperatures, Proc. Combust. Inst., 27 (1999) 219-227.

[32] M.U. Alzueta, M. Borruey, A. Callejas, Á. Millera, R. Bilbao, An experimental and modeling study of the oxidation of acetylene in a flow reactor, Combust. Flame, 152 (2008) 377-386.

[33] M. Abián, C. Esarte, Á. Millera, R. Bilbao, M.U. Alzueta. Oxidation of acetylene-ethanol mixtures and their interaction with NO, Energy Fuels, 22 (2008) 3814-3823.

[34] M. Abián, J. Giménez-López, R. Bilbao, M.U. Alzueta, Effect of different concentration levels of CO_2 and H_2O on the oxidation of CO: Experiments and modeling, Proc. Combust. Inst., 33 (2011) 317-323.

[35] B. Sirjean, R. Fournet, P.A. Glaude, F. Battin-Leclerc, W. Wang, M.A. Oehlschlaeger, Shock tube and chemical kinetic modeling study of the oxidation of 2,5-dimethylfuran, J. Phys. Chem. A 117 (2013) 1371-1392.

[36] J. Appel, H. Bockhorn, M. Frenklach, Kinetic modeling of soot formation with detailed chemistry and physics: laminar premixed flames of C2 hydrocarbons, Combust. Flame 121 (2000) 122-136.

[37] H. Richter, S. Granata, W.H. Green, J.B. Howard, Detailed modeling of PAH and soot formation in a laminar premixed benzene/oxygen/argon low-pressure flame. Proc. Combust. Inst. 30 (2005) 1397-1405.

[38] N.A. Slavinskaya, U. Riedel, S.B. Dworkin, M.J. Thomson, Detailed numerical modeling of PAH formation and growth in non-premixed ethylene and ethane flames, Combust. Flame 159 (2012) 979-995.

[39] V. Chernov, M.J. Thomson, S.B. Dworkin, N.A. Slavinskaya, U. Riedel, Soot formation with C1 and C2 fuels using an improved chemical mechanism for PAH growth, Combust. Flame 161 (2014) 592-601.

[40] H. Jin, A. Frassoldati, Y. Wang, X. Zhang, M. Zeng, Y. Li, F. Qi, A. Cuoci, T. Faravelli, Kinetic modeling study of benzene and PAH formation in laminar methane flames, Combust. Flame 162 (2015) 1692-1711.

[41] N.A. Slavinskaya, P. Frank, A modelling study of aromatic soot precursors formation in laminar methane and ethene flames, Combust. Flame 156 (2009) 1705-1722.

[42] A. D'Anna, A. Violi, A. D'Alessio, Modeling the rich combustion of aliphatic hydrocarbons, Combust. Flame 121 (2000) 418-429.

[43] C. Cavallotti, D. Polino, A. Frassoldati, E. Ranzi, Analysis of some reaction pathways active during cyclopentadiene pyrolysis, J. Phys. Chem. A 116 (2012) 3313-3324.

[44] M. Sirignano, M. Conturso, A. D'Anna, Effect of furans on particle formation in diffusion flames: An experimental and modeling study, Proc. Combust. Inst. 35 (2015) 525-532.

Figures

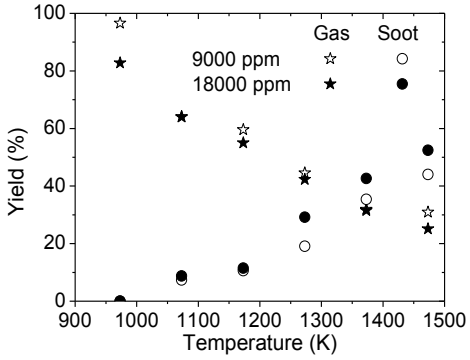

Fig. 1. Soot and gas yields, as a function of temperature, in the pyrolysis of 9000 and 18000 ppm of 2-MF.

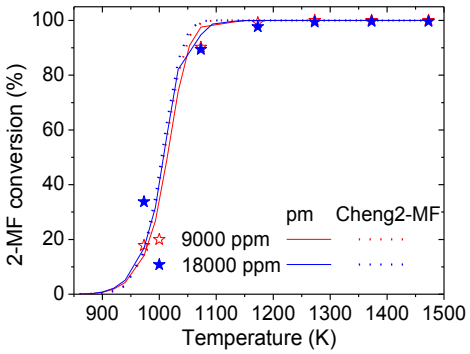

Fig. 2. Experimental (symbols) and calculated (lines) 2-MF conversion, as a function of temperature, and for different inlet 2-MF concentrations. Solid line: proposed model (pm), dot line: model of Cheng et al. [20] (Cheng2-MF).

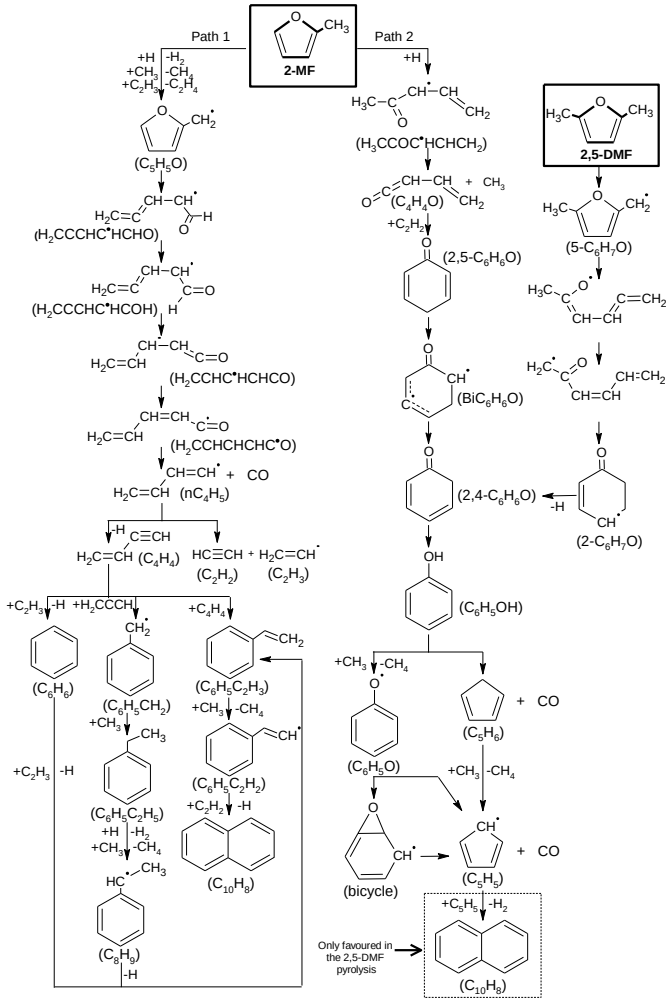

Fig. 3. Reaction flux diagram for 2-MF pyrolysis at 1000 K (fuel consumption of approximately 50 %). The main path for the 2,5-DMF pyrolysis, for approximately 50 % of fuel consumption, is also shown for discussion.

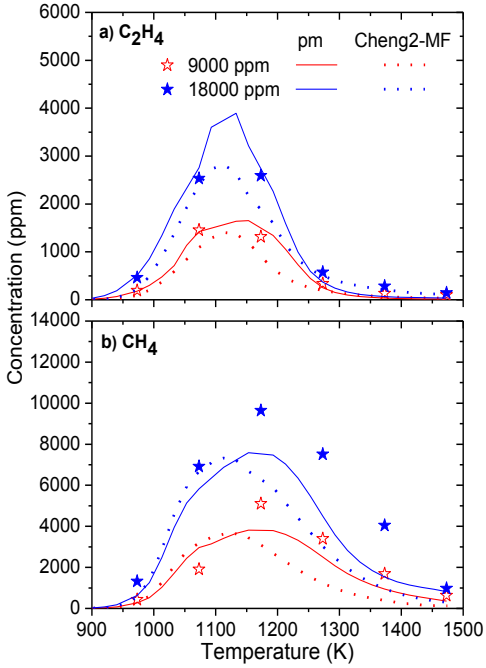

Fig. 4. Experimental (symbols) and calculated (lines) concentration profiles of ethylene and methane, as a function of temperature, for 9000 and 18000 ppm of 2-MF. Solid line: proposed model (pm), dot line: model of Cheng et al. [20] (Cheng2-MF).

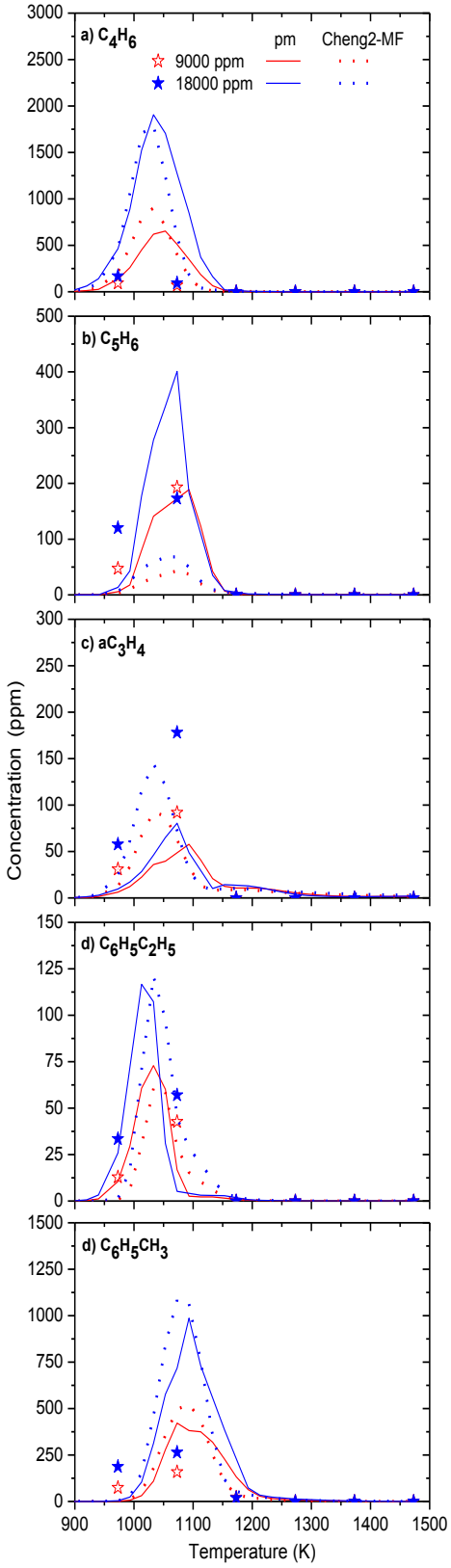

Fig. 5. Experimental (symbols) and calculated (lines) concentration profiles of the minor gases quantified in this work as a function of temperature, for 9000 and 18000 ppm of 2-MF. Solid line: proposed model (pm), dot line: model of Cheng et al. [20] (Cheng2-MF).

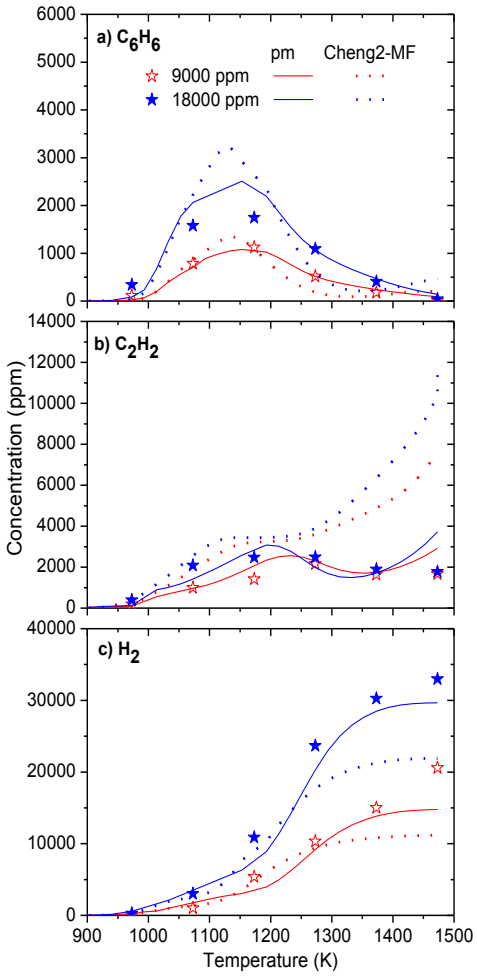

Fig. 6. Experimental (symbols) and calculated (lines) concentration profiles of benzene, acetylene and hydrogen, as a function of temperature, for 9000 and 18000 ppm of 2-MF. Solid line: proposed model (pm), dot line: model of Cheng et al. [20] (Cheng2-MF).

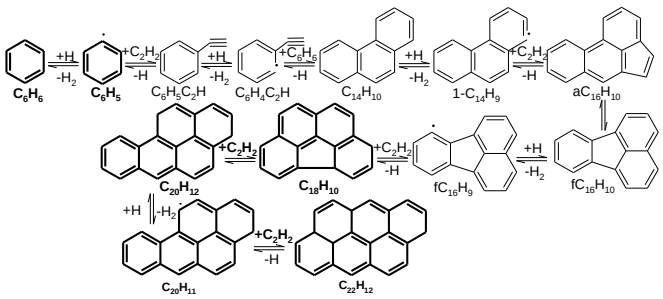

Fig. 7. Reaction sequence involved in the benzene and acetylene consumption at high temperatures. Bold species are the main paths for their consumptions in this reaction sequence. See Table S1 in Supplementary Material for the names of the structures.

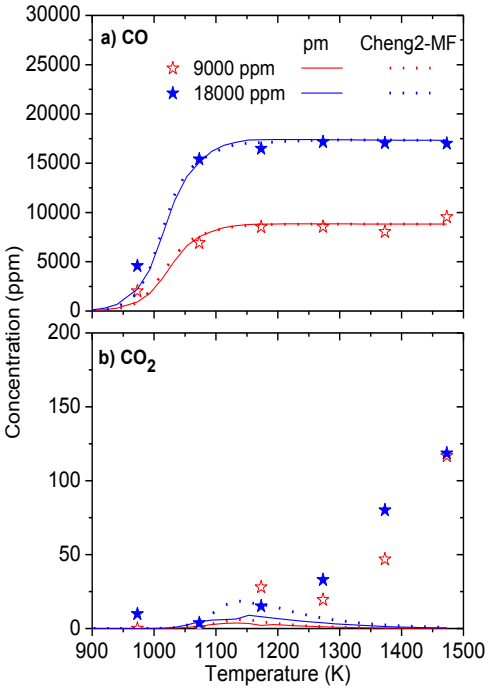

Fig. 8. Experimental (symbols) and calculated (lines) concentration profiles of CO and CO_2, as a function of temperature, for 9000 and 18000 ppm of 2-MF. Solid line: proposed model (pm), dot line: model of Cheng et al. [20] (Cheng2-MF).

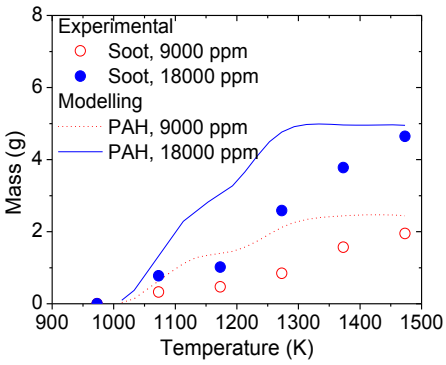

Fig. 9. Comparison of the experimental soot mass with the sum of the calculated PAH mass by the proposed model, in the pyrolysis of 9000 and 18000 ppm of 2-MF, from 975 to 1475 K.

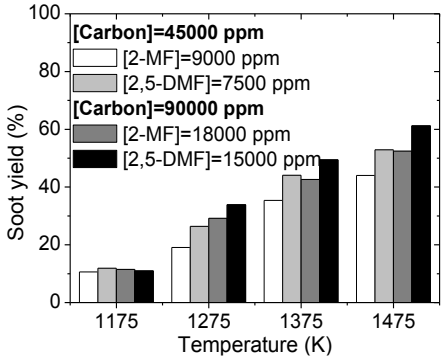

Fig. 10. Comparison of soot yield obtained in the 2-MF (9000 and 18000 ppm) and 2,5-DMF (7500 and 15000 ppm) [24] pyrolysis, from 1175 to 1475 K, for an inlet total carbon amount of 45000 and 90000 ppm, and t_r=4168/T(K).

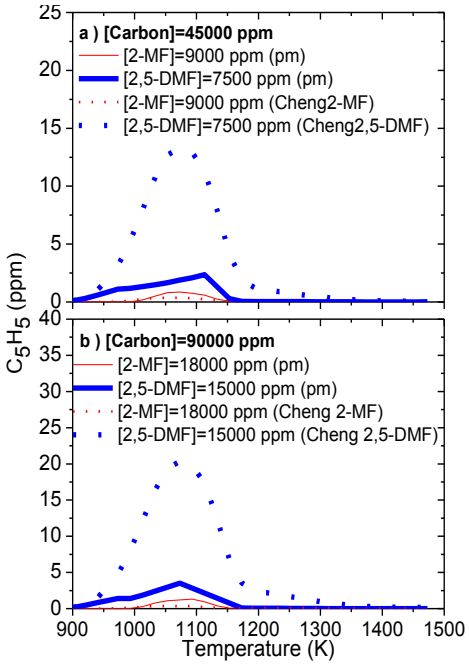

Fig. 11. Calculated concentration profiles of cyclopentadienyl radicals, as a function of temperature, for an inlet total carbon amount of 45000 and 90000 ppm ([2-MF]=9000 and 18000 ppm and [2,5-DMF]=7500 and 15000 ppm [24]). Calculations are performed with the proposed model and the Cheng2-MF [20] and Cheng2,5-DMF [26] models.

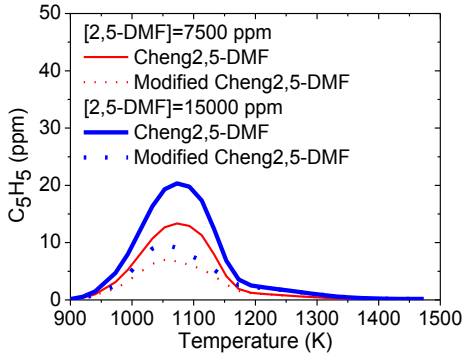

Fig. 12. Effect of the $C_5H_6 + C_5H_5 \rightleftarrows C_6H_6 + nC_4H_5$ reaction rate on the calculated C_5H_5 radicals concentration using the Cheng2,5-DMF model [26].

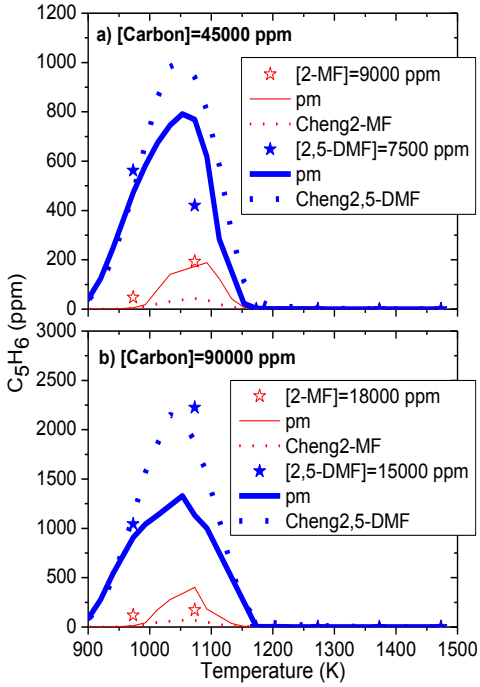

Fig. 13. Experimental (symbols) and calculated (lines) concentration profiles of cyclopentadiene, as a function of temperature, for the pyrolysis of 2-MF (9000 and 18000 ppm) and 2,5-DMF (7500 and 15000 ppm) [24], for an inlet total carbon amount of 45000 and 90000 ppm. Calculations are performed with the proposed model and the Cheng2-MF [20] and Cheng 2,5-DMF [26] models.